International Journal of Extreme Manufacturing

PAPER • **OPEN ACCESS**

Creep feed grinding induced gradient microstructures in the superficial layer of turbine blade root of single crystal nickel-based superalloy

To cite this article: Qing Miao *et al* 2021 *Int. J. Extrem. Manuf.* **3** 045102

OPEN ACCESS
IOP Publishing | IMMT
International Journal of Extreme Manufacturing
Int. J. Extrem. Manuf. 3 (2021) 045102 (14pp)
https://doi.org/10.1088/2631-7990/ac1e05

Creep feed grinding induced gradient microstructures in the superficial layer of turbine blade root of single crystal nickel-based superalloy

Qing Miao[1,2], Wenfeng Ding[1,*], Jiuhua Xu[1], Lijie Cao[3], Hongcai Wang[3], Zhen Yin[2], Chenwei Dai[2] and Weijie Kuang[1]

[1] National Key Laboratory of Science and Technology on Helicopter Transmission, Nanjing University of Aeronautics and Astronautics, Nanjing 210016, People's Republic of China
[2] College of Mechanical Engineering, Suzhou University of Science and Technology, Suzhou 215009, People's Republic of China
[3] Institute for Materials, Ruhr-Universität Bochum, Bochum 44801, Germany

E-mail: dingwf2000@vip.163.com

Received 9 June 2021, revised 22 July 2021
Accepted for publication 16 August 2021
Published 30 August 2021

Abstract

The service performance of the turbine blade root of an aero-engine depends on the microstructures in its superficial layer. This work investigated the surface deformation structures of turbine blade root of single crystal nickel-based superalloy produced under different creep feed grinding conditions. Gradient microstructures in the superficial layer were clarified and composed of a severely deformed layer (DFL) with nano-sized grains (48–67 nm) at the topmost surface, a DFL with submicron-sized grains (66–158 nm) and micron-sized laminated structures at the subsurface, and a dislocation accumulated layer extending to the bulk material. The formation of such gradient microstructures was found to be related to the graded variations in the plastic strain and strain rate induced in the creep feed grinding process, which were as high as 6.67 and 8.17×10^7 s^{-1}, respectively. In the current study, the evolution of surface gradient microstructures was essentially a transition process from a coarse single crystal to nano-sized grains and, simultaneously, from one orientation of a single crystal to random orientations of polycrystals, during which the dislocation slips dominated the creep feed grinding induced microstructure deformation of single crystal nickel-based superalloy.

Keywords: gradient microstructure, creep feed grinding, single crystal nickel-based superalloy, dislocation

1. Introduction

Nickel-based superalloys are widely employed in extreme environments to manufacture complex components in the aero-engine and gas turbine industries due to their high thermal stability, high corrosion resistance and high strength at elevated temperatures [1–3]. Grinding is the main material removal process currently used to achieve final dimensional accuracy, profile accuracy, and surface integrity for these safety critical industrial applications [4–10]. However, due to the complex thermo-mechanical interaction between the grinding tools and the workpiece, severe plastic deformation (SPD) always takes place in the superficial layer of the workpieces, usually leading to local alterations of the microstructure (e.g. grain refinement [11]) and the material

* Author to whom any correspondence should be addressed.

properties (e.g. work hardening [12, 13]). Understanding these alterations and the underlying formation mechanism has been one of the hot topics of previous studies because of their significant effects on the surface integrity which determines the fatigue life, fracture, and tribological properties of nickel-based superalloy components [14].

For this reason, numerical investigations are dedicated to clarifying the effects of mechanical grinding on the workpiece microstructure and material properties at the micro and nanoscale. For example, Ding *et al* [15] examined the subsurface metallurgical alteration of the ground groove of K424 cast nickel-based superalloy produced by creep feed grinding. A crystal lattice composed of the γ, γ' and γ'' phases was observed with moderate plastic deformation and distortion (up to 30 μm in thickness). High work hardening (up to 46% above the bulk hardness) was found in the workpiece superficial layer. Curtis *et al* [16] detected the cross-section of a Udimet 720 nickel-based superalloy after grinding and found a microstructural deformation in the superficial layer with a depth of about 10 μm and some limited thermal softening of up to 10% (below the bulk hardness). This change in the microstructure of nickel-based superalloys owes to the high thermal energy and high mechanical deformation during grinding, whose competing influence determines the transition between hardening and softening in material properties. Furthermore, under a given machining condition, the white layer, which appears featureless and white under an optical microscope, can form in the machined surface. It is usually detrimental to the fatigue life of the machined workpiece because of its hard and brittle nature. A full exploration on such a white layer was conducted by Liao *et al* [17] who studied in detail the formation mechanism, microstructure, and mechanical properties of the white layer of a S135H nickel-based superalloy. It was indicated that the deterioration of the white layer to material properties was attributed to the dissolution of the γ' strengthening phase, although the grain refinement, which was beneficial for improving material performance to some extent, can be obtained within the white layer.

However, it is worth noting that mechanical grinding has been proved as an effective way to modify material properties by introducing refined grains to the workpiece surface. As presented by Ding *et al* [18], a gradient microstructure (i.e. surface nano-laminated structure, deformation twinned structure, and severely deformed structure) of a Hastelloy C-22HS nickel-based superalloy could be produced by mechanical grinding. By virtue of micro-pillar compression tests, the yield strength of about 1650 MPa for both the nano-laminated structure and the deformation twinned structure was achieved, which was around 3.7 times greater than that of the bulk material. In addition, Liu *et al* [19] reported an ultra-hard and ultrastable nano-laminated structure (about 6.4 GPa at 504 °C) induced by high-rate shear deformation during the grinding of a polycrystalline nickel alloy. It was further found that the dislocation activities determined the formation mechanism of such a special structure [20].

Interestingly, it can be found in the above analysis that mechanical grinding can enhance material properties by grain refinement, but it can also degrade the service performance of a workpiece under high temperature and stress conditions by inducing local detrimental modifications. For such a paradox, a deep understanding is of utmost importance to control the material properties via grain refinement due to grinding.

It is noted that the single crystal nickel-based superalloy grows from a single grain and eliminates the grain boundaries thoroughly [21]. Therefore, it is capable of withstanding higher thermal and mechanical loads than a polycrystalline superalloy. This makes single crystal nickel-based superalloy one of the key materials manufacture the turbine blade roots that work under extremely high temperature and high pressure. However, such a single crystal alloy is very sensitive to stress concentration during grinding [22]. Significant efforts have been devoted to use mechanical grinding to fabricate special structures capable of tailoring the high temperature performance of polycrystalline nickel-based superalloys [18, 23]. Nevertheless, studies of grinding induced surface alterations have rarely been reported for single crystal nickel-based superalloys. Hence, two major questions remain unanswered: (a) how does the grinding induced surface alteration behave in microstructures, and (b) does mechanical grinding benefit the material performance via grain refinement.

This work aims to address these questions. A single crystal nickel-based superalloy was chosen as the workpiece material in the present study. The workpiece material was subjected to the profile grinding of one turbine blade root. The depth-dependent gradient microstructure evolution was examined by transmission electron microscopy (TEM). In particular, the transition process from a single crystal to polycrystalline grains in the superficial layer of the machined single crystal nickel-based superalloy was revealed and the underlying deformation mechanism was analyzed.

2. Experimental procedures

2.1. Materials and creep feed grinding parameters

The single crystal nickel-based superalloy used in the study was designed to have a volume fraction of γ' precipitates of about 70%. The chemical composition of this alloy is given in table 1. The alloy was manufactured using the directionally solidified casting technique, followed by a heat treatment regime: 1290 °C/1 h + 1300 °C/2 h + 1315 °C/4 h, air cooling +1120 °C/4 h, air cooling +870 °C/32 h, air cooling [24].

The creep feed profile grinding process was carried out on a computer numerical control machining center modeled PROFIMAT MT408 with a vitrified microcrystalline alumina abrasive wheel (5SG80F45A, 400 × 127 × 10 mm^3), as shown in figure 1. The abrasive wheel was profiled by a diamond roller dresser during grinding to ensure the workpiece dimensional and profile accuracy. A 5% water-based emulsion was used as the coolant. Workpieces were prepared with the dimensions of 21 (length) × 16 (width) × 15 (height) mm^3. In addition, two groups of grinding parameters were chosen to produce the blade root samples, whose total stock allowances were designed as 2.63 mm, as shown in table 2. In particular, the surface roughness after grinding was below 0.8 μm and the profile accuracy was about 10 μm.

Table 1. Chemical components of the single crystal nickel-based superalloy used in the present study.

Elements	Cr	Co	Mo	C	Ta	Nb	Re	Al	Hf	Ni
wt.(%)	4.3	9	2	0.006	7.5	0.55	2	5.6	0.1	Bal.

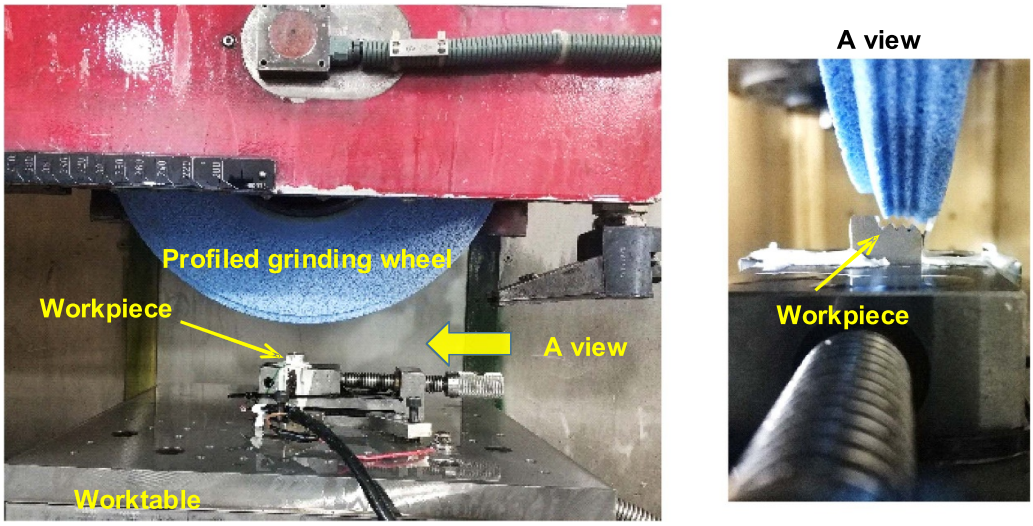

Figure 1. Experimental setup for the profile grinding of the turbine blade root.

Table 2. The parameters used in the creep feed grinding of the turbine blade root.

Group No.	Grinding stages	Grinding tests No.	Grinding speed v_s (m s^{-1})	Workpiece speed v_w (mm min^{-1})	Grinding depth a_p (mm)
I	Rough grinding	1	25	240	1.50
		2	35	150	1.00
	Finish grinding	3	35	180	0.13
II	Rough grinding	1	25	240	1.50
		2	35	420	1.00
	Finish grinding	3	35	600	0.13

2.2. Microstructure characterization

After grinding, the blade root samples were cut by electrical discharge machining both parallel and perpendicular to the workpiece feed direction. Then, these samples were mechanically polished and further processed using an ion beam. The overall cross-sectional microstructures of the blade root samples were analyzed by an electron back scatter diffraction (EBSD) and a scanning electron microscope (SEM). To study the nano-sized structures, a lamella of less than 100 nm thick was obtained from the workpiece superficial layer using focused ion beam (FEI Helios G4 CX). Meanwhile, the lamella microstructure was detected via a TEM (FEI Tecnai FP 5026 operated at 200 kV) equipped with an energy dispersive x-ray spectrometer (EDS).

3. Results

3.1. SEM overviews

For simplicity in characterization, the sample coordinates are defined as normal direction (ND), transversal direction (TD), and longitudinal direction (LD), as shown in figure 2. It is reported that the grinding loads of the root peak region are larger than those of the root valley region during blade root profile grinding [25, 26]. Therefore, the lamella in the root peak region, which is located in the middle of blade root sample, was chosen for TEM observation because the materials in the root peak regions experienced more significant plastic deformation than those in the root valley regions [25, 26].

In the superficial layer of the blade root produced by group I, as shown in figure 3, there was no visible defect on the workpiece cross-section (TD-ND plane). For the sample produced by group II, dendritic structures inside the bulk material were observed clearly on the TD-ND plane, as displayed in figure 4(a). In figure 4(b), which is the magnification micrograph of Region A marked in figure 4(a), a deformed layer (DFL) near the ground surface was observed and extended to a depth of about 5 μm. In particular, the ultrafine, featureless structure was identified by SEM when the depth from the surface was below 1 μm. While plastic deformation was obvious in a depth range of 1–2 μm. That is, the grids composed of γ' precipitates and γ channels showed an apparent bending. The

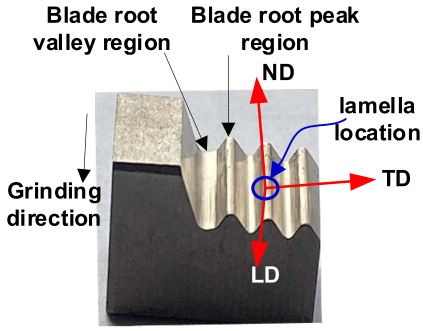

Figure 2. The blade root sample after grinding.

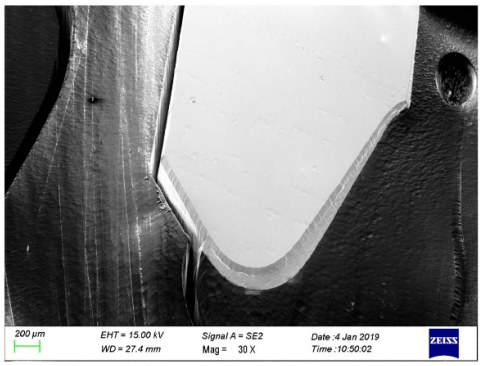

Figure 3. Cross-sectional SEM observation of sample I (TD-ND plane).

bending degree of these grids decreased with less deformed structures (figure 4(b)). When the depth exceeded 5 μm, the microstructure feature was the same as that in the bulk material (Region B shown in figure 4(c).). Such a microstructure with gradient deformation was also observed in figure 4(d), which presents the microstructure on the LD-ND plane.

Moreover, EBSD was carried out on the TD-ND plane with a scanning step of 1 μm, as shown in figure 5. For the blade root produced by grinding group I (figure 5(a)), several grains with the sizes of less than 2 μm were observed near the ground surface. These grains show different orientations which differ from those of the bulk material. However, this microstructure feature was not detected on the sample produced by grinding group II, as displayed in figure 5(b), even with an EBSD scanning step as low as 0.06 μm. But it is certain that grinding changed the microstructure in the superficial layer. The variation in the grain orientation of the bulk material (Yellow regions in figures 5(a) and (b)) can be attributed to the difference between the grain growth direction and the preferred orientation.

3.2. TEM observations of sample I

To further reveal the microstructure feature in the superficial layer, TEM characterization was performed using the above-mentioned samples. As shown in figure 6, some predominant 3 μm thick deformed structures were found in the superficial layer of sample I. In the topmost surface layer of about 1 μm thick, the plastic deformation was so severe that the grids composed of γ' and γ phases were indistinct. While in the depth range of 1–3 μm, the microstructure changes in this plastic DFL were identified in figure 6. It can be seen that significant grid sliding, distortion, and bending are induced, and some of the grids fractured or lengthened. In depths greater than 3 μm, the grid shape recovered from deformation though a large number of dislocations formed in this region. Thus, according to the distinct microstructural features, the superficial layer at different depths can be divided into the following three regions: dislocation accumulated layer (DAL), DFL, and severely deformed layer (SDL). Two regions (i.e. Region I and Region II) in figure 6 were examined at nanoscale, and were analyzed in section 3.2.3 below.

3.2.1. Microstructure of the DAL (depth > 3 μm). In the DAL, as shown in figure 7, deformed structures induced by grinding are characterized by dislocation morphology. In this region, small plastic deformation near the unaffected bulk material first attracts dislocation multiplication and movement. Then, the dislocation density increases sharply with the increasing plastic strain. Meanwhile, abundant dislocation lines and tangles are trapped within the γ' phases, as shown in figure 7(a). Moreover, many dislocations aggregate around the γ phases. By increasing the dislocation multiplication, movement, aggregation and interaction, dense walls of dislocation can form inside the grains. These dislocation walls can split one γ' phase into several parts, which is supposed to be the primary behavior that creates new grain boundaries. The selected area diffraction (SAED-1) in figure 7(b) shows a clear and sharp crystal lattice in the DAL, indicating that the material inside the DAL still possesses a single crystal structure even if this region suffers from plastic strain during grinding.

3.2.2. Microstructure of the DFL (depth: 1–3 μm). In the depth range of 1–3 μm (figure 8), a high density of dislocations was detected and the γ'-precipitates and γ-channels bent along the grinding direction. Thus, the grids consisting of γ'-precipitates and γ-channels seem to have lengthened as a bending rectangle, as shown in figure 8(a). In the vicinity of the DFL, close to the severely DFL, the γ'-precipitates with a generally decreasing thickness (e.g. from 200 to 500 nm) were observed until they fractured. This is caused by the further development of dislocations inside γ'-precipitates, which promotes the splitting action with the increasing deformation degree of the workpiece material in the DFL. The SAED-2 image in figure 8(b) shows the rotating diffraction spots and demonstrates that the single crystal structure is likely to be twisted or the new grains form with small misorientation angles.

3.2.3. Microstructure of the severely DFL (depth < 1 μm). Microstructures in the region of less than 1 μm from the surface (figure 9) showed the small grains that seem to have formed from fragmentations of the γ'-precipitates and γ-channels. Furthermore, these fine grains (less than 200 nm in size) were uniformly distributed in this layer (figures 9(a)

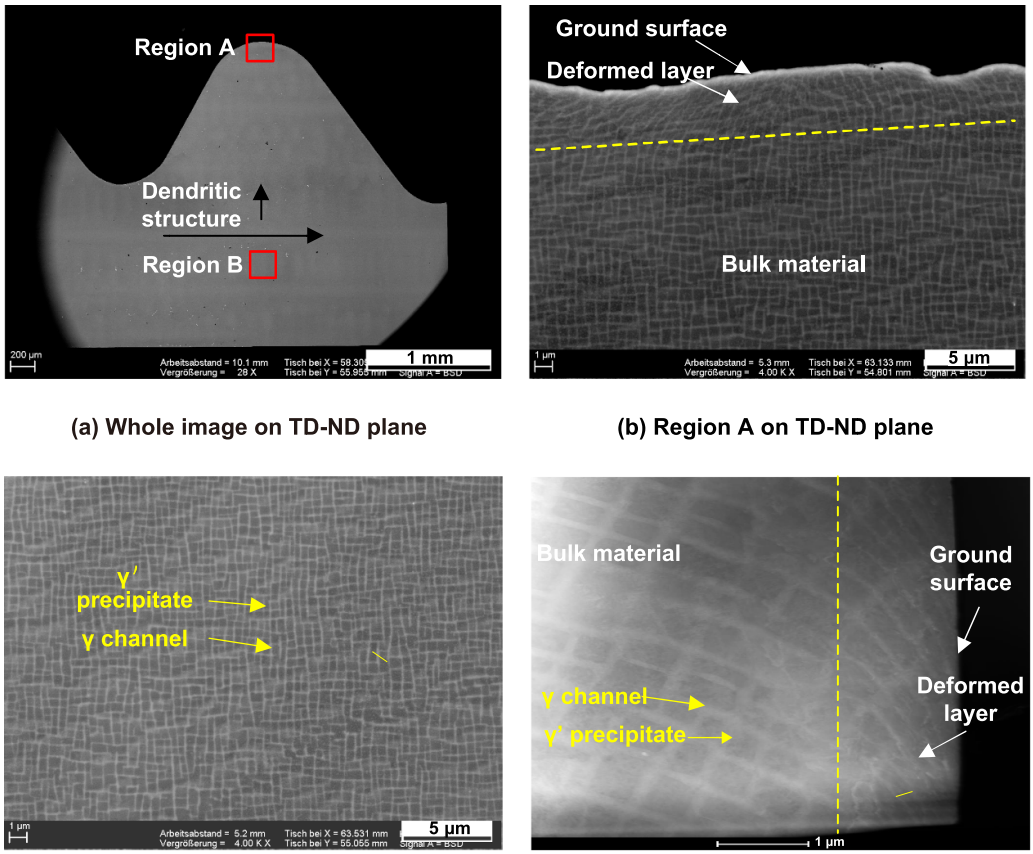

(a) Whole image on TD-ND plane (b) Region A on TD-ND plane

(c) Region B on TD-ND plane (d) Microstructure on LD-ND plane

Figure 4. Cross-sectional SEM observation of blade root sample II.

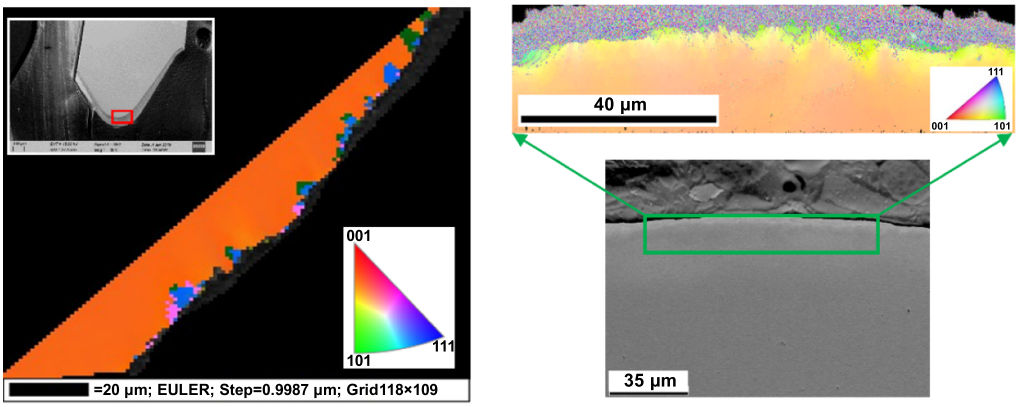

(a) Sample I (b) Sample II

Figure 5. Cross-sectional EBSD maps of the blade root sample on the TD-ND plane.

and (c)). The electron diffraction patterns of almost continuous rings observed in figures 9(b) and (d) suggest that the polycrystalline structures probably formed in the topmost layer of the single crystal nickel-based superalloy, indicative of higher shear strain level in the SDL compared with that in the DFL. However, there are still some preferential orientations which exist with moderate intensity differences in the diffraction rings, implying the formation of low angle grain boundaries [27].

3.3. TEM observations of sample II

3.3.1. Microstructure in the superficial layer. By means of the similar TEM characterization method, the deformation structures on the TD-ND plane of sample II were investigated, as displayed in figure 10. Two layers (i.e. DFL and SDL) with clear boundaries were found (figure 10(a)). The typical microstructures in the DFL include dislocations and submicron grains induced by these dislocations, as shown in figure 10(b). The dislocation walls still exist within the submicron-sized

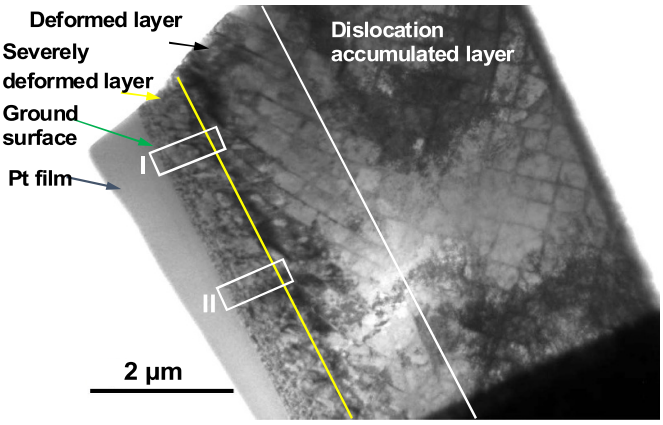

Figure 6. Cross-sectional TEM image showing the overall microstructure in blade root sample I on the TD-ND plane.

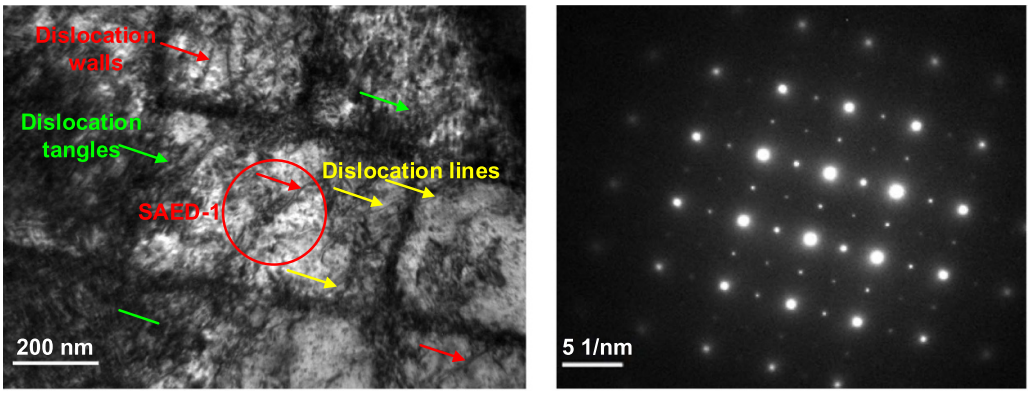

(a) Dislocation structures (b) SAED-1

Figure 7. Cross-sectional TEM images of the microstructure at about 5 μm from the ground surface in sample I on the TD-ND plane.

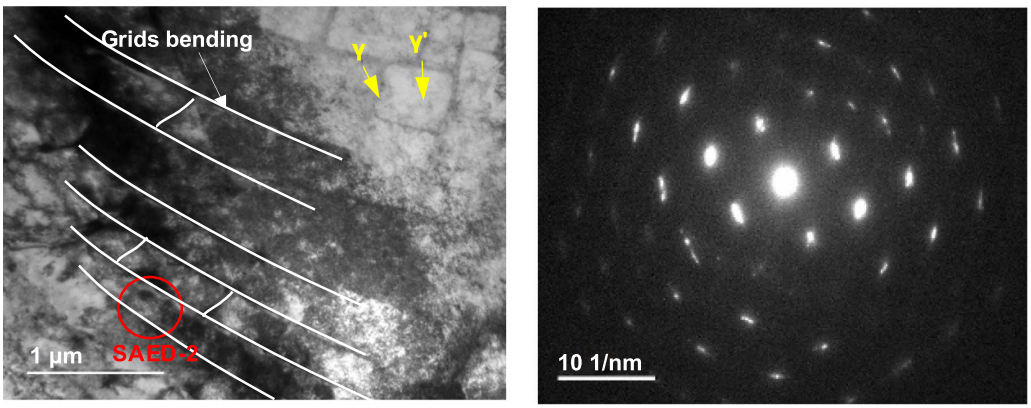

(a) Deformation of γ' and γ phases (b) SAED-2

Figure 8. Cross-sectional TEM images of the microstructure at about 2 μm from the ground surface in sample I on the TD-ND plane.

nucleation, which can further split the grains and form the boundaries of submicron grains if massive deformations are exerted continuously. In the SDL, equiaxed nanograins smaller than 100 nm can be observed and are uniformly distributed. Figure 10(c) shows the electron diffraction patterns of circle rings, indicating the nanograins with random orientations. Interestingly, some white particles at nanoscale in the topmost surface were observed, as shown in figure 10(b). EDS analysis of point A (white particle) and point B (nanograin), which are marked in figure 10(b), was performed to detect the elemental composition, as shown in figure 11. It can be seen that the O and Al contents of point *A* are much higher than those of point *B*, implying that the white particles might be oxides. It has been reported that in the machined surface, the oxygen cavitation/pore can be induced near the γ' phase [17]. This indicates that the γ' phase had a smaller oxide fraction than

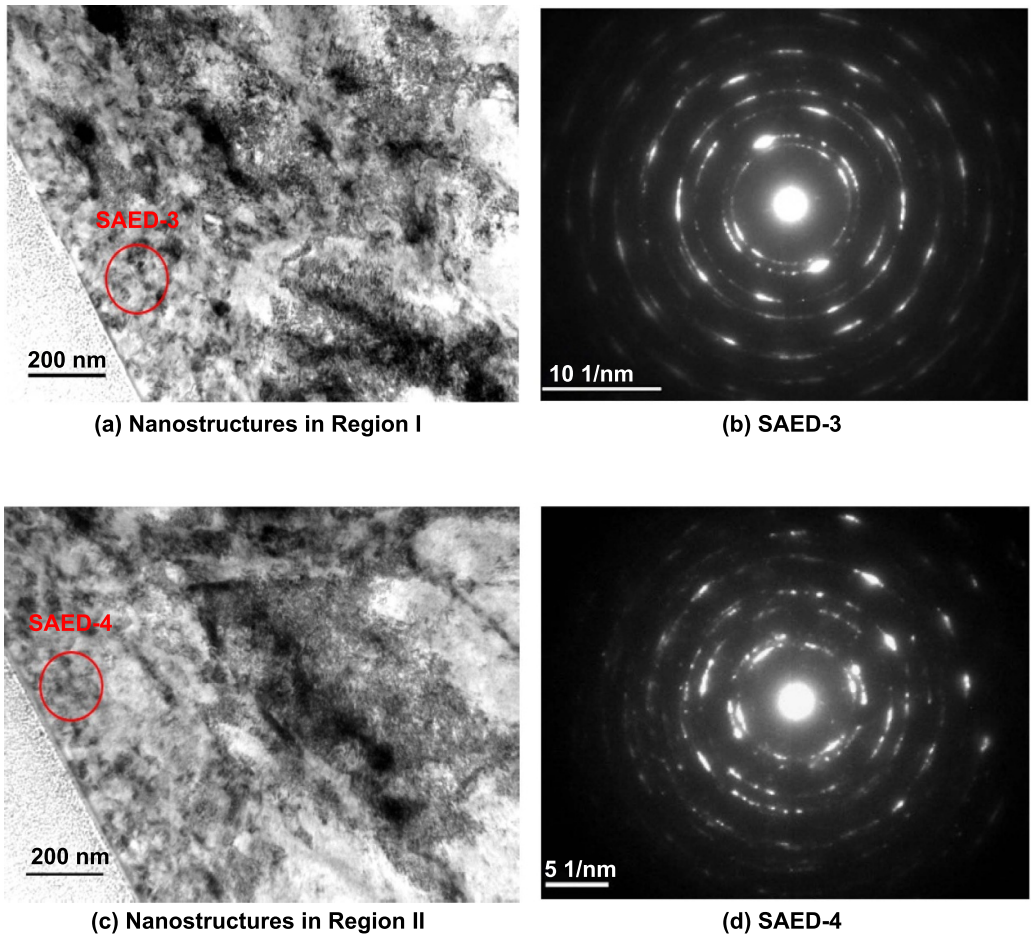

(a) Nanostructures in Region I (b) SAED-3

(c) Nanostructures in Region II (d) SAED-4

Figure 9. Cross-sectional TEM images of the microstructure at about 0.2 μm from the ground surface in sample I on the TD-ND plane.

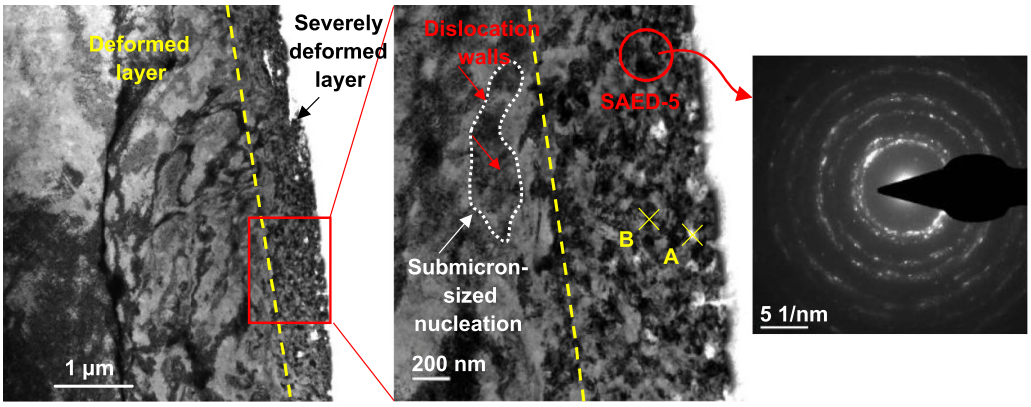

(a) Whole (b) Regional (c) SAED-5

Figure 10. Cross-sectional TEM images of the deformation microstructure on the TD-ND plane in sample II.

the γ phase. In other words, the O elements came from the bulk material. However, in the present study, it is highly likely that the O elements originated from the air or the alumina grains because these white particles were distributed in the edge region of the ground surface, and the high strain and heat during grinding can easily cause oxidation between alumina grains and workpiece materials [28].

3.3.2. Nanotwins in the superficial layer. The nano-twined structure shown in figure 12 can be grasped in the superficial layer of blade root sample II on the LD-ND plane. This section of the ground layer presents the morphology of nanograins and submicron grains clearly, as displayed in the bright/dark field images (figures 12(a) and (b)). Nanotwins deeper than 10 nm from the surface were detected (figure 12(c)), which

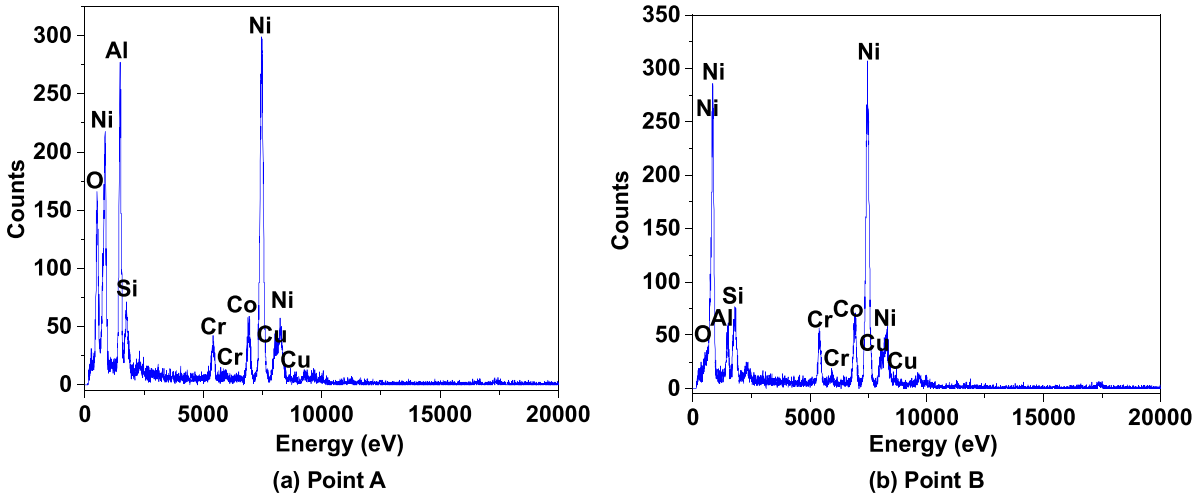

Figure 11. EDS analysis on points A and B marked in figure 10(b).

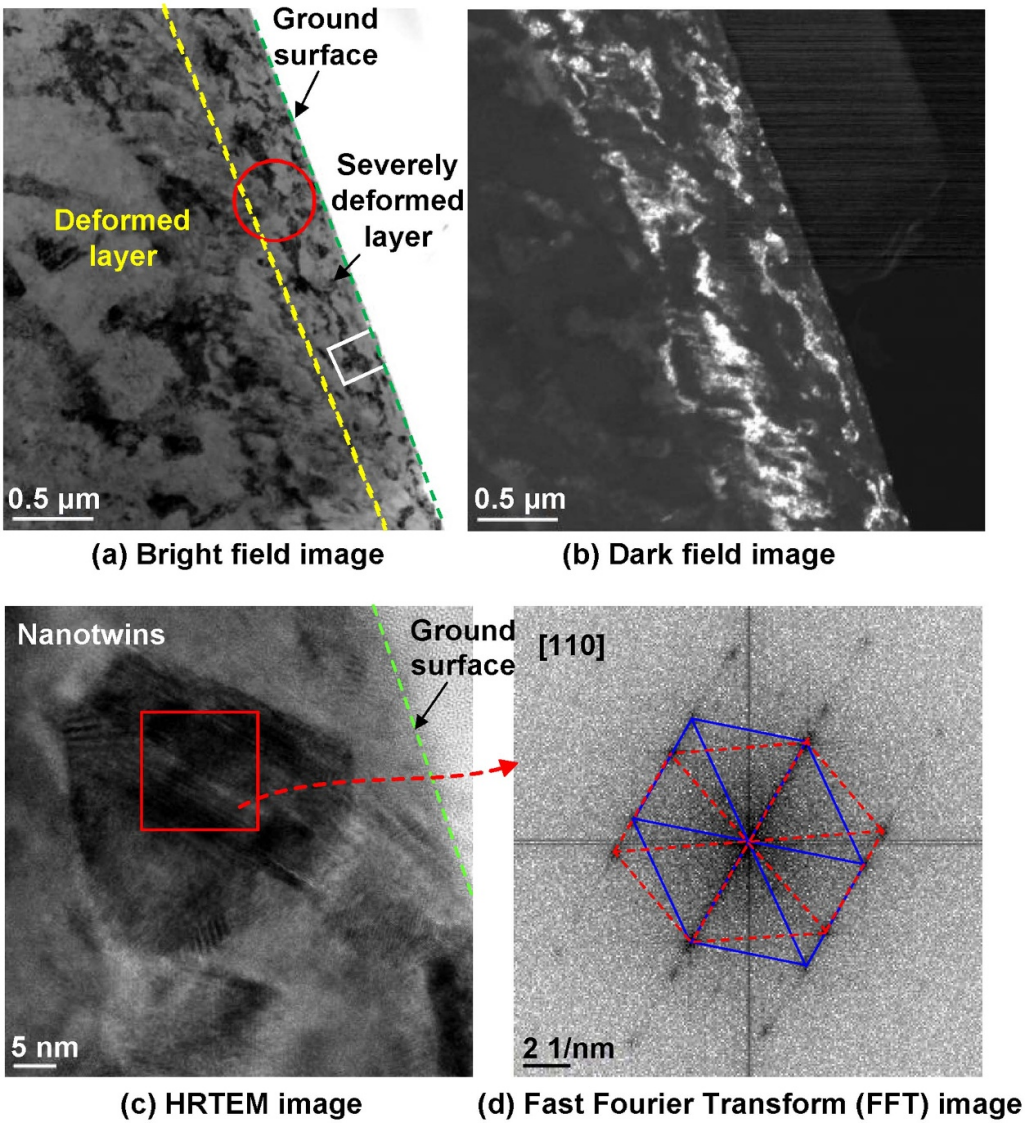

Figure 12. TEM observation of nanotwins in the superficial layer of blade root sample II on the LD-ND plane.

have equiaxed crystal and sharp twin boundaries. The nano-twined structure was approximately 30 nm in size. A symmetrical crystal plane was obtained via fast Fourier transform analysis, as shown in figure 12(d).

It has been demonstrated that nano-twined structures have excellent physical properties, such as very high thermal stability and superior strength retention as compared with fine-grained metals [29–31]. Unfortunately, this unique structure is difficult to find in other regions of the sample though massive endeavors were made in the present study, suggesting that few nanotwins are produced within the blade root workpiece under the present grinding conditions. Liu *et al* [19] reported that lower twin boundary energies favor the formation of nanoscale twins. Thus, twinning is easily achieved in face-centered cubic metals with low stacking fault energies (SFEs), while it is significantly difficult to produce twinning in metals with high SFEs [29]. For the single crystal nickel-based alloy, it is still an open question why the twinning cannot be induced abundantly in the superficial layer after grinding.

4. Discussion

The microstructures formed by plastic deformation induced grain refinement consist of dislocation, submicron grain, and nanograin. These microstructures can be fabricated by means of various methods, including cold rolling [32], mechanical attrition [33], and mechanical grinding [34]. It has been proven that, the strain, strain rate, and strain gradient induced by the mechanical treatments play a crucial role in the grain refinement process [35]. Therefore, to analyze the grain refinement mechanism in the current study, the strain and strain rate during grinding were estimated based on the Merchant theory in metal cutting mechanics [36]. Assuming the removed material in unit volume only comes into contact with one abrasive grain, that is, the shear strain ε in the cutting zone is induced by a single grain in unit time. Thus, the shear strain ε and strain rate $\dot{\varepsilon}$ can be calculated by [37, 38]:

$$\varepsilon = \frac{\cos\alpha_n}{\sin\varphi_n \cos(\varphi_n - \alpha_n)} \tag{1}$$

$$\dot{\varepsilon} = \frac{\lambda v_s \cos\alpha_n \sin\varphi_n}{a_e \cos(\varphi_n - \alpha_n)} \tag{2}$$

$$a_e \approx 0.5 a_{g\max} = 0.5\left[\frac{4}{C\cdot N_d}\cdot\frac{v_w}{v_s}\cdot\left(\frac{a_p}{d_s}\right)^{1/2}\right]^{1/2} \tag{3}$$

where α_n is the abrasive grain rank angle; φ_n is the shear angle according to [39, 40]; λ is the aspect ratio of the shear zone, ranging from 6 to 12 [41]; a_e is the thickness of the shear zone, equivalent to half of the maximum undeformed chip thickness $a_{g\max}$; C is a constant related to the abrasive rank angle; N_d is the active abrasive grain number; and d_s is the wheel diameter.

The parameters used in the current study are listed in table 3. Substituting the above parameters into equations (1)–(3), the shear strain and strain rate can be evaluated for the finish grinding process. It can be found that, the ground surface endures shear deformation with a strain of up to 6.67 and a high strain rate of about $8.17 \times 10^7\ \mathrm{s}^{-1}$. The strain rates are around three orders of magnitude higher than that induced by cutting [17]. In addition, due to the multiple grinding processes of the blade root, the accumulated strain can form a large strain gradient within the superficial layer. Therefore, these conditions are beneficial for dislocation generation, significantly elevating the dislocation density in the workpiece.

Table 3. Calculation of strain and strain rate in the shear zone during grinding.

Group No. Grinding stages	I Finish grinding	II Finish grinding
Grain rank angle α_n	$-35°$	$-35°$
Shear angle φ_n	12°	10°
Constant C	1.428	1.428
Active grain number N_d	6.1 mm^{-2}	6.1 mm^{-2}
Grinding wheel diameter d_s	387 mm	387 mm
Aspect ratio of shear zone λ	7	9
Maximum undeformed chip thickness $a_{g\max}$	0.85 μm	1.55 μm
Shear strain	5.78	6.67
Strain rate	$7.89 \times 10^7\ \mathrm{s}^{-1}$	$8.17 \times 10^7\ \mathrm{s}^{-1}$

4.1. Formation of submicron-sized grains

The above observations in figures 7–12 indicate that the dislocation activities determine the microstructure alternation of the ground layer. In other words, to accommodate more dislocations, many lamellar-shaped structures formed, deriving from the cell blocks and dislocation walls, as demonstrated in figure 13. With increasing plastic strains, more lamellar-shaped structures were induced with decreasing thickness when more boundaries formed in such structures (figure 13(a)). These lamellar-shaped structures were further split into several parallel ones by the increasing dislocation walls, which were perpendicular to the lamellar boundaries (figure 13(b)). Therefore, the boundary spacing reduced, and the submicron grains nucleated and grew (figure 13(c)), which might have originated from the subdivided parts of one lamellar-shaped structure. This process was realized by a continuous increase of dislocation accumulation into the boundaries. Furthermore, due to the ununiformed distribution of extended boundaries, the width and length of submicron grains were not identical, having averaged values of 66 and 158 nm, respectively, with an aspect ratio of about 2.5 (figures 13(c)–(e)). Compared to the nucleation of submicron grains (figure 13(c)), these relatively coarse submicron grains contained comparable aspect ratios in grain sizes but more

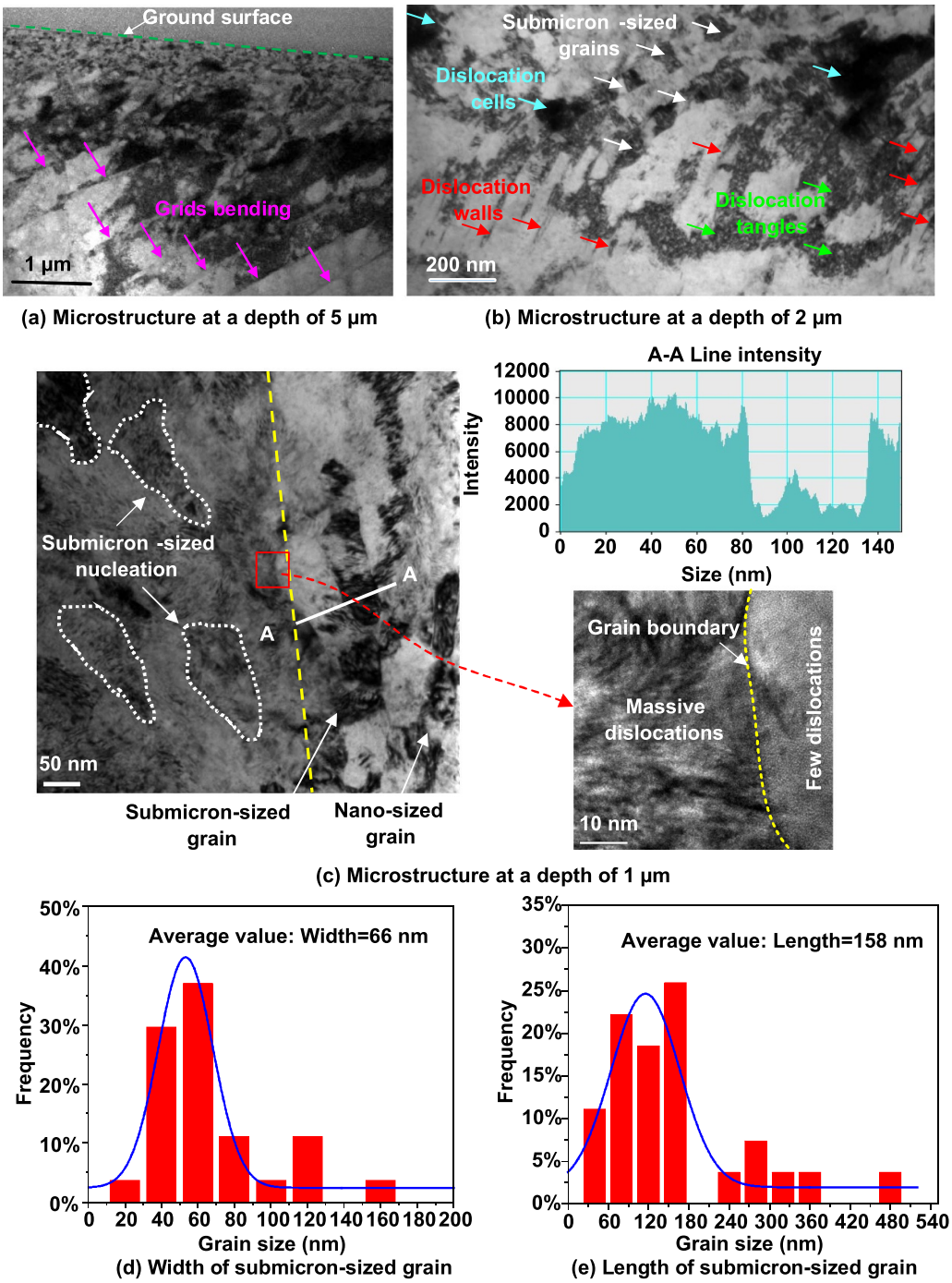

Figure 13. Formation of submicron-sized grains in the ground layer of blade root sample II on the LD-ND plane.

clear boundaries and lower contents of dislocations. However, the further refinement of grains can benefit from these loose dislocations within the submicron grains.

The above-mentioned process might be the primary mechanism for reducing grain size and generating submicron grain boundaries in the ground layer of single crystal nickel-based superalloy. According to [42], the formation of one grain is closely related to the grain boundary misorientation. Under the increasing strains, the adjacent boundaries start to slip at different crystal slip systems when the grain boundary misorientation increases to a certain extent. If more dislocations are continuously incorporated into the grain boundaries under larger strains, the grain morphologies and textures can change with higher boundary misorientations [43]. The grain subdivision can be reached under such conditions. It can be stated that the grain boundary misorientation results from the micron splitting of a single crystal nickel-based superalloy.

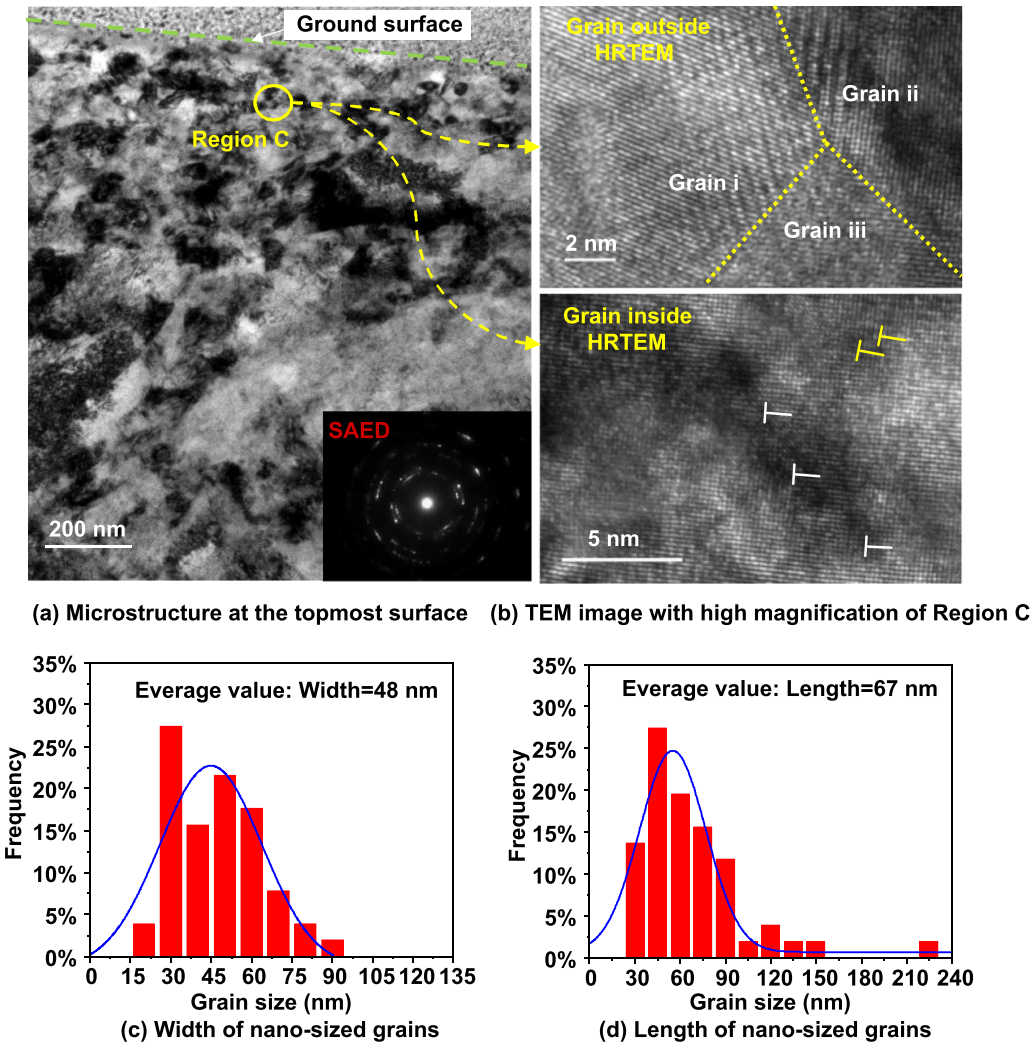

Figure 14. Formation of nano-sized grains in the ground layer of blade root sample I on the TD-ND plane.

4.2. Formation of nano-sized grains

The topmost surface of the workpiece experienced the most SPD, as evaluated by table 3. Under such conditions, the generation of dislocations and grain boundaries can be enhanced significantly, which provides a unique opportunity for the formation of nano-sized grains and texture evolution. Massive dislocations formed due to the high strain induced by the grinding process. The balance between dislocation generation and annihilation was not be achieved because there was insufficient time resulting from the high strain rate. This leads to a pop-in phenomenon of the dislocation density in the topmost surface, as demonstrated by Zhang *et al* [44]. Moreover, to keep the whole crystal continuity and deformation compatibility, the storage of geometrically necessary dislocations is promoted due to the large strain gradient [45]. Therefore, the creep feed grinding of a single crystal nickel-based superalloy in the present study can efficiently facilitate the generation and accumulation of dislocations. This contributes to the formation of the low angel grain boundaries with a high density. To absorb the accumulated dislocations, different dislocation structures, including dislocation lines, dislocation tangles, dislocation walls, and dislocation cells, developed sequentially and then nucleated massively, resulting in the growth of grain boundaries, as described in section 4.1.

In turn, to reduce the stored energy, these dislocation structures gradually formed grain boundaries with low angles. The formation of nanograins is the continuous and strong interaction between dislocations and submicron grain boundaries. Such a fragmentation process of the submicron structures can be observed in figure 14, where there are clear shapes of nanograins and triple junctions (figure 14(b)). The presence of nanograins with an aspect ratio of 1 (48 nm width and 67 nm length) indicates the formation of equiaxed crystals. Ding *et al* [18] reported that the nanograins tend to be equiaxed and dislocation-free. However, some dislocations with different Burgers vectors ('T' symbols in figure 14(b)) were observed around the grain boundaries in the present study. The limited dislocation activities suggest that the nanograins are not defect-free, and the chance for surface grain division and further refinement still exists.

Analogous formation mechanisms of surface nanograins can be found in the deformation of Cu [46] and Al alloys [27]

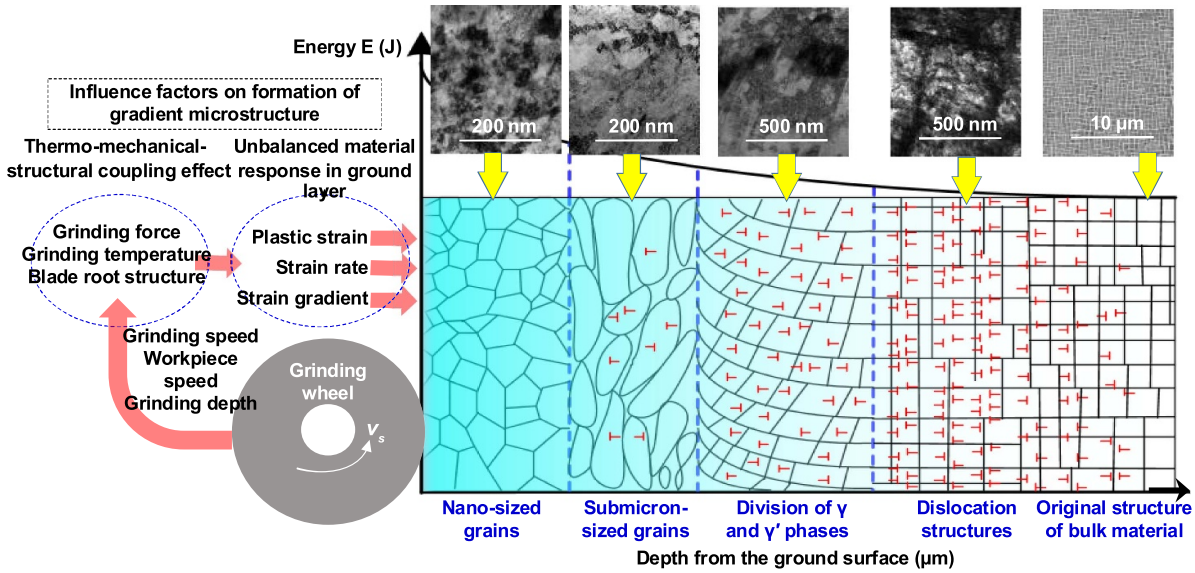

Figure 15. Transition process of a single crystal to polycrystalline grains in the ground layer of single crystal nickel-based superalloy.

where the interactions between dislocations and grain boundaries play the predominating role. However, in the ground layer of single crystal nickel-based superalloy, the main difference lies in the unique formation process of its nanograins. This can occur because the grids composed of γ and γ' phases are divided into numerous fragmentations by grain boundaries deriving from intensive dislocation structures, while the grain orientations are created and re-distributed in such a process.

4.3. Transition of a single crystal to polycrystalline grains

In general, the main mechanisms for accommodating the plastic deformation of materials include dislocation slip and deformation twinning. Based on the above analysis, it can be determined that the dislocation activity dominates the surface microstructure evolution produced by creep feed grinding of single crystal nickel-based superalloy. In particular, due to the relatively low temperature generated during creep feed grinding (less than 120 °C [47]), temperature has a weak influence on dislocation and, therefore, is not considered in the present study. For metals with low SFEs, dislocation slip is usually suppressed, whereas deformation twinning becomes the favorable mechanism [48]. While for metals with high SFEs, dislocation is induced initially at special low-index crystal planes [49]. For the single crystal nickel-based superalloy, dislocation is most likely to slip at the {111} crystal plane, which has small critical stresses due to its relatively high SEFs [50]. Thus, the dislocation slip can be activated in different directions even at one crystal plane. This provides the crucial possibility for subdividing one originally coarse single crystal into thousands of randomly oriented polycrystalline nanograins.

The evolution characteristics of the surface gradient microstructures of single crystal nickel-based superalloy induced by creep feed grinding can be illustrated with three steps, as shown in figure 15:

Step I: When surface plastic deformation occurs, the structure of a single crystal begins to accumulate dislocations at the micro level, and then the crystal twisting and rotation at the macro level happens with an adjustment of the orientation of a single crystal in the ground layer.

Step II: The single crystal is subdivided into the submicron grains with low angel boundaries by means of dislocation accumulation in both the γ-channels and γ'-precipitates.

Step III: With increased strain, the submicron grains are refined further with decreasing grain size, increasing grain misorientation, and the shape changes from unregular to equiaxed.

The evolution process of the gradient microstructure in the superficial layer is essentially the transition not only from a coarse single crystal to nano-sized grains, but also from one orientation of a single crystal to the random orientations of polycrystals, of which the structure formation is governed mainly by the dislocation activities. This is different from a previous study on polycrystalline Inconel 718 alloy, where the initial coarse grains are subdivided by mechanical twinning [51].

In addition, many investigations have found that the gradient structured materials, with nano-sized grains in the surface layer and coarse grains in the inner core, present unique mechanical behaviors, such as interstitial free steel with gradient microstructures having high yield strength [52] and copper with gradient microstructures showing 10 times higher tensile strength than that without gradient microstructures [53]. This indicates that by creating gradient microstructures in the superficial layers of such alloys, it can become a potential and effective approach to further enhance the service performance of a turbine blade root. However, due to the complicated thermo-mechanical-structural coupling effect during profile grinding (figure 15), the changes of strain, strain rate and strain gradient are significant and thus difficult to predict. How to qualitatively correlate the plastic deformation to

the thermo-mechanical-structural coupling effect by means of adjusting the grinding parameters (e.g. grinding speed, workpiece speed and grinding depth), is critical for actively controlling the formation of gradient microstructures.

5. Conclusions

(a) Creep feed grinding produces gradient deformation structures in the surface layer of turbine blade root of single crystal nickel-based superalloy, including nano-sized grains (48–67 nm), submicron-sized grains (66–158 nm), micron-sized laminated structures and dislocation structures.
(b) The gradient microstructures within the superficial layer are attributed to the notable variations in plastic strains (up to 6.67) and strain rates (up to 8.17×10^7 s^{-1}) induced by the creep feed grinding process from the ground surface to the bulk material of the single crystal nickel-based superalloy.
(c) The evolution of gradient microstructures in the ground layer takes place during the transition from coarse single crystal to nano-sized grains as well as from one orientation of single crystal to random orientation of polycrystal. The structure deformation primarily depends on the dislocation slip and the deformation twinning as a supplement.

Acknowledgments

This work was financially supported by the National Natural Science Foundation of China (Nos. 51921003, 51775275 and 51905363), the Natural Science Foundation of Jiangsu Province (No. BK20190940), the National Major Science and Technology Projects of China (No. 2017-VII-0002-0095), and the Six Talents Summit Project in Jiangsu Province (No. JXQC-002).

ORCID iD

Wenfeng Ding https://orcid.org/0000-0001-7687-4319

References

[1] Klocke F, Soo S L, Karpuschewski B, Webster J A, Novovic D, Elfizy A, Axinte D A and Tönissen S 2015 Abrasive machining of advanced aerospace alloys and composites *CIRP Ann.-Manuf. Technol.* **64** 581–604
[2] Sun J Y, Yang S and Yuan H 2021 Assessment of thermo-mechanical fatigue in a nickel-based single-crystal superalloy CMSX-4 accounting for temperature gradient effects *Mater. Sci. Eng.* A **809** 140918
[3] Miao Q, Ding W F, Kuang W J and Yang C Y 2021 Grinding force and surface quality in creep feed profile grinding of turbine blade root of nickel-based superalloy with microcrystalline alumina abrasive wheels *Chin. J. Aeronaut.* **34** 576–85
[4] Chen J J, Fu Y C, Qian N, Jiang H F, Ching C Y, Ewing D and Dai C W 2021 Investigation on cooling behavior of axially rotating heat pipe in profile grinding of turbine blade slots *Appl. Therm. Eng.* **182** 116031
[5] Aspinwall D K, Soo S L, Curtis D T and Mantle A L 2007 Profiled superabrasive grinding wheels for the machining of a nickel based superalloy *CIRP Ann.-Manuf. Technol.* **56** 335–8
[6] Li H N, Zhao Y J, Cao S Y, Chen H, Wu C Q, Qi H, Sun X, Wang H X, Li C H and Liu G Y 2021 Controllable generation of 3D textured abrasive tools via multiple-pass laser ablation *J. Mater. Process. Technol.* **295** 117149
[7] Fan Z H, Tian Y B, Zhou Q and Shi C 2020 A magnetic shear thickening media in magnetic field–assisted surface finishing *Proc. Inst. Mech. Eng.* B **234** 1069–72
[8] Chen J J, Fu Y C, Qian N, Ching C Y, Ewing D and He Q S 2021 A study on thermal performance of revolving heat pipe grinding wheel *Appl. Therm. Eng.* **182** 116065
[9] Tian Y B, Li L G, Han J G, Fan Z H and Liu K 2021 Development of novel high-shear and low-pressure grinding tool with flexible composite *Mater. Manuf. Process.* **36** 479–87
[10] Tian Y B, Li L G, Liu B, Han J G and Fan Z H 2020 Experimental investigation on high-shear and low-pressure grinding process for Inconel718 superalloy *Int. J. Adv. Manuf. Technol.* **107** 3425–35
[11] Liao Z R, la Monaca A, Murray J, Speidel A, Ushmaev D, Clare A, Axinte D and M'Saoubi R 2021 Surface integrity in metal machining—part I: fundamentals of surface characteristics and formation mechanisms *Int. J. Mach. Tools Manuf.* **162** 103687
[12] Xu Y C, Gong Y D, Wang Z X, Wen X L, Yin G Q, Zhang H and Qi Y 2021 Experimental study of Ni-based single-crystal superalloy: microstructure evolution and work hardening of ground subsurface *Arch. Civ. Mech. Eng.* **21** 43
[13] Wang Y S, Xiu S C and Zhang S N 2021 Microstructure evolution and crystallographic slip modes during grind hardening in TC21 titanium alloy *Surf. Coat. Technol.* **417** 127211
[14] Thakur A and Gangopadhyay S 2016 State-of-the-art in surface integrity in machining of nickel-based super alloys *Int. J. Mach. Tools Manuf.* **100** 25–54
[15] Wenfeng D, Jiuhua X, Zhenzhen C, Honghua S and Yucan Y C 2010 Grindability and surface integrity of cast nickel-based superalloy in creep feed grinding with brazed CBN abrasive wheels *Chin. J. Aeronaut.* **23** 501–10
[16] Curtis D T, Soo S L, Aspinwall D K and Mantle A L 2016 Evaluation of workpiece surface integrity following point grinding of advanced titanium and nickel based alloys *Proc. CIRP* **45** 47–50
[17] Liao Z R, Polyakov M, Diaz O G, Axinte D, Mohanty G, Maeder X, Michler J and Hardy M 2019 Grain refinement mechanism of nickel-based superalloy by severe plastic deformation—mechanical machining case *Acta Mater.* **180** 2–14
[18] Ding J, Li Q, Li J, Xue S, Fan Z, Wang H and Zhang X 2018 Mechanical behavior of structurally gradient nickel alloy *Acta Mater.* **149** 57–67
[19] Liu X C, Zhang H W and Lu K 2013 Strain-induced ultrahard and ultrastable nanolaminated structure in nickel *Science* **342** 337–40
[20] Liu X C, Zhang H W and Lu K 2015 Formation of nano-laminated structure in nickel by means of surface mechanical grinding treatment *Acta Mater.* **96** 24–36
[21] Reed R C 2006 *The Superalloys: Fundamentals and Applications* (Cambridge: Cambridge University Press)
[22] Jichun X, Jiarong L and Shizhong L 2010 Surface recrystallization in nickel base single crystal superalloy DD6 *Chin. J. Aeronaut.* **23** 478–85
[23] Swaminathan S *et al* 2005 Large strain deformation and ultra-fine grained materials by machining *Mater. Sci. Eng.* A **410–1** 358–63

[24] Xiong X H, Quan D M, Dai P D, Wang Z P, Zhang Q X and Yue Z F 2015 Tensile behavior of nickel-base single-crystal superalloy DD6 *Mater. Sci. Eng.* A **636** 608–12
[25] Miao Q, Li H N and Ding W F 2020 On the temperature field in the creep feed grinding of turbine blade root: simulation and experiments *Int. J. Heat Mass Transfer* **147** 118957
[26] Miao Q, Ding W F, Kuang W J and Xu J H 2020 Tool wear behavior of vitrified microcrystalline alumina wheels in creep feed profile grinding of turbine blade root of single crystal nickel-based superalloy *Tribol. Int.* **145** 106144
[27] Chen Y X, Yang Y Q, Feng Z Q, Huang B and Luo X 2017 Surface gradient nanostructures in high speed machined 7055 aluminum alloy *J. Alloys Compd.* **726** 367–77
[28] Wu C J, Guo W C, Li R, Zhao Y D and Zhou Q Z 2020 Thermal effect on oxidation layer evolution and phase transformation in grinding of Fe-Ni super alloy *Mater. Lett.* **275** 128072
[29] Cheng Z, Zhou H F, Lu Q H, Gao H J and Lu L 2018 Extra strengthening and work hardening in gradient nanotwinned metals *Science* **362** eaau1925
[30] Lu K 2016 Stabilizing nanostructures in metals using grain and twin boundary architectures *Nat. Rev.* **1** 16019
[31] Sun L G, Wu G, Wang Q and Lu J 2020 Nanostructural metallic materials: structures and mechanical properties *Mater. Today* **38** 114–35
[32] Wang M, Jiang Y B, Li Z, Xiao Z, Gong S, Qiu W T and Lei Q 2021 Microstructure evolution and deformation behaviour of Cu-10 wt%Fe alloy during cold rolling *Mater. Sci. Eng.* A **801** 140379
[33] Liu X M, Nakatani M, Gao H L, Sharma B, Pan H J, Fu Z R, Li X F, Ameyama K and Zhu X K 2021 Effect of staking fault energy on deformation mechanisms in Cu and Cu-30% Zn alloy with gradient structure obtained by SMAT *J. Alloys Compd.* **865** 158863
[34] Li C, Cui W F and Zhang Y S 2017 Surface self-nanocrystallization of $\alpha + \beta$ titanium alloy by surface mechanical grinding treatment *Met. Mater. Int.* **23** 512–8
[35] Lu K 2014 Making strong nanomaterials ductile with gradients *Science* **345** 1455–6
[36] Merchant M E 1945 Mechanics of the metal cutting process II. Plasticity conditions in orthogonal cutting *J. Appl. Phys.* **16** 318–24
[37] Oxley P L B 1989 *The Mechanics of Machining: An Analytical Approach to Assessing Machinability* (Chichester: Ellis Horwood Limited)
[38] Malkin S and Guo C S 2008 *Grinding Technology: Theory and Applications of Machining with Abrasives* 2nd edn (New York: Industrial Press)
[39] Yan L, Li X K, Jiang F, Zhou Z X and Rong Y M 2009 Research on microscopic grain-workpiece interaction in grinding through micro-cutting simulation, part 2: factorial study *Adv. Mater. Res.* **76–78** 15–20
[40] Ohbuchi Y and Obikawa T 2003 Finite element modeling of chip formation in the domain of negative rake angle cutting *J. Eng. Mater. Technol.* **125** 324–32
[41] Jin T 1999 *Fundamental Research on High Efficiency Deep Grinding Technology* (Shenyang: Northeastern University)
[42] Bay B, Hansen N, Hughes D A and Kuhlmann-Wilsdorf D 1992 Overview no. 96 evolution of f.c.c. deformation structures in polyslip *Acta Metall. Mater.* **40** 205–19
[43] Hughes D A and Hansen N 1997 High angle boundaries formed by grain subdivision mechanisms *Acta Mater.* **45** 3871–86
[44] Zhang B and Shim V P W 2010 Effect of strain rate on microstructure of polycrystalline oxygen-free high conductivity copper severely deformed at liquid nitrogen temperature *Acta Mater.* **58** 6810–27
[45] Yang M X, Pan Y, Yuan F P, Zhu Y T and Wu X L 2016 Back stress strengthening and strain hardening in gradient structure *Mater. Res. Lett.* **4** 145–51
[46] Li W L, Tao N R and Lu K 2008 Fabrication of a gradient nano-micro-structured surface layer on bulk copper by means of a surface mechanical grinding treatment *Scr. Mater.* **59** 546–9
[47] Rowe W 2017 Temperatures in grinding—a review *J. Manuf. Sci. Eng.* **139** 121001
[48] Lu K, Lu L and Suresh S 2009 Strengthening materials by engineering coherent internal boundaries at the nanoscale *Science* **324** 349–52
[49] Lu L 2004 Ultrahigh strength and high electrical conductivity in copper *Science* **304** 422–6
[50] Laplanche G, Wieczorek N, Fox F, Berglund S, Pfetzing-Micklich J, Kishida K, Inui H and Eggeler G 2018 On the influence of crystallography and dendritic microstructure on micro shear behavior of single crystal Ni-based superalloys *Acta Mater.* **160** 173–84
[51] Luo J T, Yu W L, Xi C Y, Zhang C X and Ma C H 2019 Preparation of ultrafine-grained GH4169 superalloy by high-pressure torsion and analysis of grain refinement mechanism *J. Alloys Compd.* **777** 157–64
[52] Wu X L, Jiang P, Chen L, Zhang J F, Yuan F P and Zhu Y T 2014 Synergetic strengthening by gradient structure *Mater. Res. Lett.* **2** 185–91
[53] Fang T H, Li W L, Tao N R and Lu K 2011 Revealing extraordinary intrinsic tensile plasticity in gradient nano-grained copper *Science* **331** 1587–90